NUMERICAL MODEL OF MICROWAVE BACKSCATTERING AND EMISSION FROM TERRAIN COVERED WITH VEGETATION

P. Ferrazzoli, L.Guerriero, and D. Solimini
Dipartimento di Ingegneria Elettronica, Università Tor Vergata,
Via O. Raimondo, 00173 Roma, Italy

Abstract

A computational model for estimating microwave scattering and emission from the earth's surface covered with vegetation (*MESCAM*) has been developed. The model is founded on relevant electromagnetic properties of the vegetation and of the underlying terrain and takes into account multiple scattering both within the vegetation and between vegetation and underlying soil. By selecting the appropriate scattering functions, the backscattering coefficient and the emissivity can be estimated in a wide range of frequencies, for different sensor configurations, and for a variety of terrain and vegetation characteristics.

1 Introduction

In electromagnetic research, a large effort is being devoted to the evaluation of scattering from conducting and dielectric bodies of variable shapes, sizes, and orientation with respect to the incoming wave. The purpose may be twofold. On one side, the power scattered in selected directions is sought for, using appropriate analytical and numerical techniques, once the geometrical and physical parameters of the scatterer are known (direct problem). On the other, these latter parameters are to be determined from suitable sets of scattered electromagnetic field data (inverse problem). The characteristics of scattering objects can be largely variable, from the single body of simple shape, for which analytical solutions may be appropriate, to ensembles of heterogeneous bodies, requiring an electromagnetic complex system approach. This is indeed the case when the earth's surface is involved, and, for instance, clutter evaluation is needed in terms of its physical parameters (direct problem) or remote sensing of the geophysical quantities is carried out (inverse problem).

The surface of the solid earth is composed of more or less inhomogeneous layers of soil and rocks with rough interfaces with eventually embedded stones and boulders. The surface may be bare, but, at least in temperate climates, is generally covered with vegetation, i.e., grass, bushes, trees, or crops. This is a clearly complex electromagnetic environment, whose characterization from the scattering and emitting point of view requires an appropriate and peculiar approach. First, the relevant scattering and absorbing elements must be singled out, then they must be characterized electromagnetically in a sufficiently realistic fashion, finally they must be assembled in order to

model the properties of the complex system through the interactions of the many individual elements. With the possible exception of bare rocky surfaces, at microwaves, the soil can be regarded as a lossy dielectric homogeneous half-space with rough boundary. The overlaying vegetation is modeled according to its predominant morphology, i.e. by aggregates of lossy dielectric disks or needles to represent leaves of deciduous trees or conifers, respectively, and of lossy cylinders of various diameters to model embedded, stalks, branches and trunks.

Microwave scattering from ensembles of disks, needles, and cylinders has been considered in the past [1]-[4] to model radar response of vegetation within selected ranges of sensor parameters. A comprehensive numerical model, the Microwave Emission and SCAttering Model (*MESCAM*) has also been developed by us to compute in a unified approach both the microwave backscattering coefficient and the emissivity of vegetated terrain. This model, which appears to reproduce experimental data with good accuracy, has been employed to put into relation emissivity and backscattering data measured on agricultural fields [5] and to carry out a parametric analysis of the effects of single soil and vegetation parameters on the responses of radar and radiometric sensors to crop-covered soils [6].

A feature of the model is its capability of including multiple scattering among the vegetation elements, realistically represented by disks and cylinders, as well as between the vegetation and the soil. If on one side this feature leads to computational complexity, on the other it is advantageous, since it allows careful estimates of the scattering and emission mechanisms for various ranges of frequency and incidence angle and for both the co-polar and cross-polar cases. The model is also able to compute separately the contributions from the different sources of emission and scattering, e. g., from leaves, stalks, and terrain, taking into account the corresponding multiple interactions. Hence, it provides a means to understand the importance of the various sources, and reliable guidelines in decomposing the physical structure of the vegetated surface into simple components for which the more appropriate treatment from the point of view of accuracy and computational efficiency can be devised and worked out.

This paper reports a detailed description of the numerical model, starting from some physical hypothesis on the vegetation layer and on the underlying soil. The electromagnetic characterization of the elementary layers into which the whole vegetation canopy is subdivided, is carried out through the Stokes matrix, whose elements take into account the polarized absorption and scattering properties of the single scatterers and their distribution of orientation. The doubling algorithm [7] is then applied recursively to succeeding layers to build up the global microwave scattering properties of the vegetation, and, at the end, to include the effect of the soil. Two methods of computation of the microwave emissivity, which is directly related to the bistatic scattering coefficient by the conservation of energy, are also described. Selected examples of the results obtained by our model are finally reported and discussed.

2 Physical background

The ground surface covered by vegetation is considered as an ensemble of lossy dielectric elements of simple shape, whose absorbing and scattering properties are described by appropriate analytical expressions. Thus, according to the type of vegetation, the considered elementary scatterers will be cylinders (able to model trunks, branches,

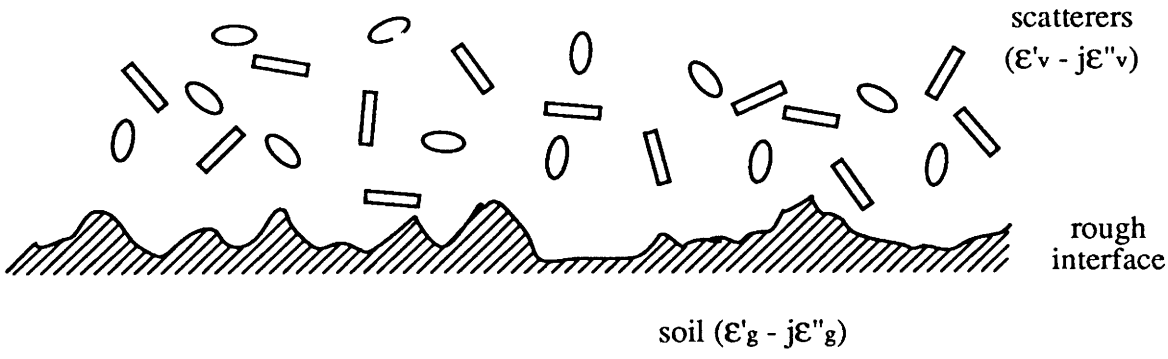

Figure 1: Model of a vegetation layer over soil.

stalks, etc.), disks to model plane leaves, and needles when tillers or conifer leaves are present. The disks, which can be of circular or elliptical shape, are obtained by flattening spheroids or ellipsoids, through the contraction of one dimension. The slab containing the ensemble of scatterers lies on a lossy dielectric homogeneous half-space (representing the terrain) with a rough interface (Fig. 1).

To characterize electromagnetically the elements of vegetation, both their permittivity and geometry are needed. The complex dielectric constant $\epsilon'_v - j\epsilon''_v$ of plant constituents is essentially controlled by water, so that an essential input is the moisture content of leaves, or branches, etc., usually given in percent by volume or by weight [8]. Once the shape of the scatterers is identified, the dimensions of the plant elements provide the dimensions of the scatterers, i.e., length, width and thickness of disks, length and diameter of needles or other cylindrical bodies. The distribution of orientation of the scatterers, and the height and density of the vegetation canopy provide further parameters needed to characterize the collective behavior of the ensemble of elements. In turn, the geometry and the dielectric constant $(\epsilon'_g - j\epsilon''_g)$ of the underlying soil are determined by the height standard deviation and correlation length of the soil surface, and by its moisture content, respectively [9].

3 Electromagnetic characterization of the canopy

Once the vegetation canopy is modelled as a layer of elementary lossy scatterers over the soil surface, the procedure requires the subdivision of the layer into elementary sub-layers, whose thickness is set by the condition that interactions among scatterers belonging to the same sub-layer are negligible. This is easily feasible in practice, since the vegetation medium is usually electromagnetically tenuous.

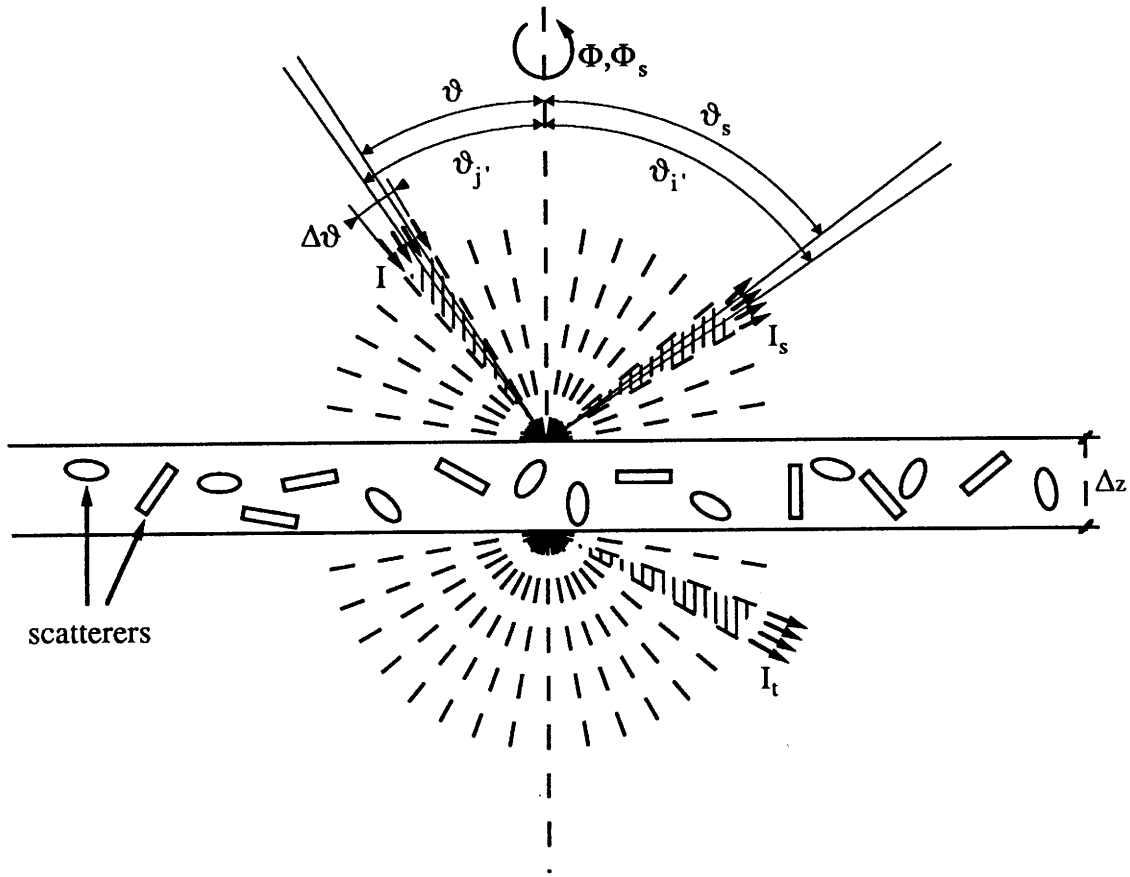

Figure 2: Discretization of off-nadir angle for an elementary sub-layer of thickness Δz. I is the incident specific intensity; I_s and I_t are specific intensities respectively scattered and transmitted by the sub-layer.

3.1 Scatter matrix computation

Two half-spaces (upper and lower) are associated with each elementary sub- layer and each half-space is subdivided into N_θ "conical shells" generated by rotation about the vertical axis of a pair of straight lines forming an angle $\Delta\theta$ (Fig. 2), which is the unit interval of the discretized off-nadir angle θ. The incidence and scattering azimuth angles are denoted by ϕ and ϕ_s, respectively. The global electromagnetic properties of the vegetation are assumed to be independent of the azimuth angle, so that, the scattering from the sub-layer depends on $\phi_s - \phi$ only. If the incidence plane is assumed to be the $\phi = 0$ plane, then the scattering pattern depends on the azimuth scattering angle ϕ_s only.

The average electromagnetic behavior of individual lossy scatterers is conveniently described by the 4×4 Stokes matrix $\mathbf{P}$ [10], which is computed according to the following steps.

- a) A pair of scattering (denoted by index i') and incidence (index j') conical shells of angular width $\Delta\theta$ around off-nadir angles $\theta_{i'}$ and $\theta_{j'}$ is considered ($1 \leq i', j' \leq N_\theta$).

- b) A pair of scattering (θ_s) and incidence (θ) off-nadir angles are considered, within the corresponding conical shells defined in a).

- c) An azimuth scattering direction ϕ_s is considered.
- d) The orientation of each scatterer is defined by the Eulerian angles α, β, γ [3].
- e) The scattering functions f_{vv}, f_{hh}, f_{vh}, and f_{hv} are computed analytically by use of formulations appropriate to the particular individual scatterer and to the considered range of frequency [11], [12], [13], [14] and, in turn, the Stokes matrix elements of the scatterer are computed.
- f) The results of computations described in e) are averaged over the range of values of α, β, γ and θ and θ_s internal to the conical shells, to compute the average Stokes matrix elements P_{pq}. These elements are relative to off-nadir scattering and incidence angular intervals indicated by indices i' and j', and to azimuth angle ϕ_s. Subscripts p and q $(p, q = 1, .., 4)$ select the scattered Stokes parameters and the incident ones, respectively.
- g) The procedure is repeated for all values of i' and j' $(1 \leq i', j' \leq N_\theta)$ and for N_ϕ discrete values of the scattering azimuth angle ϕ_s $(0 \leq \phi_s < 2\pi)$.
- h) For each ϕ_s value, an expanded $4N_\theta \times 4N_\theta$ **M** matrix is computed. Each element of this matrix represents the ratio of the $p-th$ scattered over the $q-th$ incident Stokes parameter for off-nadir directions of scattering and incidence around $\theta_{i'}$ and $\theta_{j'}$, respectively. For $p, q = 1, 2$, a matrix element represents the p-polarized power density scattered into the $i'-th$ conical shell per unit q-polarized power density incident from the $j'-th$ direction. Elements of **M** will be labelled by i and j, where $i = N_\theta \cdot (p-1) + i'$ and $j = N_\theta \cdot (q-1) + j'$.

In the hypothesis of randomly located independent scatterers, if ΔA is the element area and Δz the thickness of the sub-layer, the Stokes matrix elements P_{pq} of the volume $\Delta A \cdot \Delta z$ are proportional to the number of elements in the volume, i.e. $n \cdot \Delta A \cdot \Delta z$, where n is the number of scatterers per unit volume.

The number of intervals N_θ of the off-nadir angle is determined as the minimum value beyond which the computed σ^o stabilizes (i.e., shows variations below 0.5 dB). The same procedure is followed to select the number of intervals N_ϕ into which the azimuthal angle is subdivided. To gain some further insight into the computational effort which is required, we mention that at X-band a reasonable accuracy is obtained, in case only disks are considered, by choosing:

- $N_\theta = 9$, which corresponds to $\Delta\theta = 10^o$;
- two values of θ and θ_s for each conical shell;
- $N_\phi = 16$
- $0 \leq \alpha < \pi$ with 30^o step;
- $0 \leq \beta \leq \pi/2$ with 10^o step;
- $\gamma = 0$.

It should be noted that the elements of the Stokes matrix $\mathbf{P}$ are expressed in $m^2/sterad$ and give the ratio between scattered power densities per unit solid angle ($W/sterad$) and incident power densities per unit area (W/m^2). On the other hand, the behavior of an elementary sub-layer is suitably described by its scatter matrix $\mathbf{S}$, whose elements are dimensionless ratios between scattered and incident specific intensities ($W/m^2 \cdot sterad$). To proceed to compute the scatter matrix elements, an incident power uniformly distributed within a cone of width $\Delta\theta sin\theta d\phi$ of specific intensity I_j is assumed. The scattered power density per unit solid angle in the direction identified by i' and ϕ_s is

$$dp_{\Omega si}(\phi_s) = I_j \Delta\theta sin\theta d\phi M_{ij}(\phi_s) n \Delta A \Delta z \tag{1}$$

and the scattered specific intensity

$$dI_{si}(\phi_s) = \frac{I_j \Delta\theta sin\theta d\phi M_{ij}(\phi_s) n \Delta z}{cos\theta_s} \tag{2}$$

For every pair of incidence and scattering conical shells and for each pair of Stokes parameters, a scattering function can be defined, given by

$$S'_{ij}(\phi_s) = \frac{dI_{si}(\phi_s)}{I_j d\phi} \tag{3}$$

so that

$$S'_{ij}(\phi_s) = \frac{n \Delta z \Delta\theta sin\theta}{cos\theta_s} \cdot M_{ij}(\phi_s) \tag{4}$$

Note that in an actual situation the power comes from the upper half-space and the scattering function S'_{ij} describes scattering into the upper half-space too. Scattering towards the lower half-space can be described in a similar fashion by using a transmission function $T'_{ij}(\phi_s)$.

The scattering and transmission functions S'_{ij} and T'_{ij} are subsequently Fourier transformed with respect to ϕ_s, so that in the transformed domain they are represented by $2(N_\phi/2 + 1)$ square matrices $\mathbf{S'}_m$ and $\mathbf{T'}_m$ of dimensions $4N_\theta \times 4N_\theta$, provided N_θ is the number of intervals into which the $0 \leq \theta \leq \pi/2$ range is subdivided. Note that $S'_{ij}(-\phi_s) = S'_{ij}(\phi_s)$ and $T'_{ij}(-\phi_s) = T'_{ij}(\phi_s)$ due to the azimuthal symmetry, so that only the even terms of the Fourier series are required. If both incident and scattered specific intensities are expressed as Fourier series,

$$I_j(\phi) = \sum_m I_{jm} cos(m\phi) \tag{5}$$

$$I_{si}(\phi_s) = \sum_m I_{sim} cos(m\phi_s) \tag{6}$$

each Fourier component of I_s, i.e. I_{sim}, can be related to the corresponding component of I, i.e. I_{jm} through the relation

$$I_{sim} = S_{ijm} I_{jm} \tag{7}$$

where

$$\mathbf{S}_m = a_m \mathbf{S'}_m, \tag{8}$$

with the parameter a_m given by

$$a_m = \begin{cases} 2\pi & \text{if } m = 0 \\ \pi & \text{if } m > 0 \end{cases}$$

The Fourier components of the specific intensity traveling downward I_{tim} can be expressed in an analogous way through the corresponding components T_{ijm} of the transmission matrix.

3.2 Propagation of power in the canopy

As the incident power travels downward in the canopy, it undergoes both absorption and scattering by the lossy elements of the vegetation. To obtain the total power in the canopy, the downward scattered power, expressed by the $\mathbf{T}_m$ matrices, must be added to the fraction of undisturbed power. This is accomplished by adding the quantity $1 - K_{ej}$ to the diagonal elements of $\mathbf{T}_m$, if K_{ej} is the fraction of power traveling within the $j' - th$ conical shell for q Stokes index which undergoes extinction in the considered sub-layer. K_{ej} takes into account the effect of both absorption and scattering by the vegetation elements:

$$K_{ej} = [\sigma_{aj} + \sigma_{sj}] \cdot \frac{n\Delta z}{cos\theta} \tag{9}$$

In (9) σ_{aj} is the average absorption cross-section of the elements of vegetation for incidence direction j' and Stokes index q, and σ_{sj} is their average scattering cross section. The absorption cross section can be expressed in terms of the imaginary part of the permittivity of the elements ϵ_v'' and of dyads that depend on their shape (see, for instance, [3]), while the scattering cross section can be obtained from the scattering functions f_{pq} of the considered scatterers by

$$\sigma_{sj} = \int_0^{2\pi} \int_0^{\pi} < [f_{qq}^2(\theta_s, \phi_s) + f_{pq}^2(\theta_s, \phi_s)] > sin\theta_s d\theta_s d\phi_s \tag{10}$$

For each type of scatterer, the average, indicated by the sharp brackets, is performed over the Eulerian angles α, β, γ describing the scatterer orientation and over the θ angle interval enfolded within the $j' - th$ conical shell.

4 Electromagnetic characterization of soil

The scattering properties of the terrain are expressed by the dimensionless bistatic scattering coefficient $\sigma_g^o(\theta, \theta_s; \phi_s)$, which depends on the permittivity of the soil and on the roughness of its surface. Several models worked out for estimating scattering from a rough surface can be used (see, for instance, [15]). For the higher frequencies, i.e., for X-band and above, a geometrical optics model has been implemented, while for lower frequencies, typically at L-band, the physical optics (for low θ values) and the small perturbation (for high θ values) is used. More critical is the choice of the scattering model for the intermediate frequency range, where, in practice, the corresponding conditions of validity are more difficult to meet. The integral equation method [16] and the phase perturbation technique [17] are being tested for situations where the other solutions fail.

The models of scattering from the rough soil surface require as input data the soil moisture, and the height standard deviation and correlation length of the surface. The computed bistatic scattering coefficient $\sigma_g^o(\theta, \theta_s; \phi_s)$, is then employed to construct the Fourier scattering matrices of the soil $\mathbf{S}'_{gm}$ through the scattered specific intensity (i.e., power density per unit surface per unit solid angle)

$$dI_{si}(\phi_s) = \frac{1}{4\pi cos\theta_s} I_j \Delta\theta sin\theta d\phi \sigma^o_{gij} \tag{11}$$

The procedure is the same as the one already described for the vegetation elementary layer, leading to the computation of the $\mathbf{S}_{gm}$ matrices.

5 Combining Scattering from Different Layers

The various terms identified and defined in the preceding sections are combined as follows.

If two adjacent elementary layers are characterized by scattering and transmission matrices $\mathbf{S}_{1m}, \mathbf{T}_{1m}$ and $\mathbf{S}_{2m}, \mathbf{T}_{2m}$ respectively, the corresponding matrices of the layer composed of the two sub-layers are obtained through a matrix "doubling" [7], [3], i.e.,

$$\mathbf{S}_m = \mathbf{S}_{1m} + \mathbf{T}_{1m}\mathbf{S}_{2m}(\mathbf{1} - \mathbf{S}_{1m}\mathbf{S}_{2m})^{-1}\mathbf{T}_{1m} \tag{12}$$

and, analogously,

$$\mathbf{T}_m = \mathbf{T}_{2m}(\mathbf{1} - \mathbf{S}_{1m}\mathbf{S}_{2m})^{-1}\mathbf{T}_{1m} \tag{13}$$

By reiterating this procedure, the N sub-layers of the vegetation canopy are successively combined, and the Fourier components of the scattering and transmission matrices $\mathbf{S}_{vm}$ and $\mathbf{T}_{vm}$ of the whole canopy are computed. Finally, the contribution of the soil is included through the following matrix operation:

$$\mathbf{S}_{tm} = \mathbf{S}_{vm} + \mathbf{T}_{vm}\mathbf{S}_{gm}(\mathbf{1} - \mathbf{S}_{vm}\mathbf{S}_{gm})^{-1}\mathbf{T}_{vm} \tag{14}$$

In this way the $\frac{N_\phi}{2} + 1$ Fourier scattering matrices of the overall scattering object, i.e., soil covered with vegetation, are obtained. The number N (power of two) of elementary layers into which the whole canopy is subdivided, is selected as the minimum value beyond which the computed σ^o does not vary by more than 0.5 dB.

6 Computation of the Backscattering Coefficient

Once the total matrices $\mathbf{S}_{tm}$ are computed, the total scattering functions in the backward direction $\phi_s = \pi, \theta_s = \theta = \theta_0$, where θ_0 is the observation angle of the radar sensor, can be obtained by the Fourier series

$$S'_{ij}(\pi) = \sum_{m=0}^{N_\phi/2+1} \frac{1}{a_m} S_{tijm} cos(m\pi) \tag{15}$$

where

$$
\begin{aligned}
i &= N_\theta(p-1)+i'_0 \\
j &= N_\theta(q-1)+j'_0 \\
i'_0 &= j'_0 \\
&= Int(\frac{\theta_0}{\Delta\theta})+1
\end{aligned} \tag{16}
$$

The polarized backscattering coefficient of the observed pixel of area ΔA is finally obtained through its definition

$$
\sigma^o_{ij} = \frac{4\pi}{\Delta A}\cdot\frac{dp_{\Omega si}(\pi)}{dp_{Aj}} \tag{17}
$$

where $dp_{\Omega si}(\pi)$ is the power density per unit solid angle backscattered by area ΔA, and dp_{Aj} is the incident power per unit area. It follows that

$$
\begin{aligned}
\sigma^o_{ij} &= \frac{4\pi}{\Delta A}\cdot\frac{dI_{si}(\pi)(\Delta A cos\theta_0)}{Ij\Delta\theta sin\theta_0 d\phi} \\
&= \frac{4\pi}{\Delta\theta}\cdot(cotg\theta_0)S'_{ij}(\pi)
\end{aligned} \tag{18}
$$

It should be noted that $i=j$ in the co-polar case.

7 Computation of Emissivity

Emissivity can be computed by two different procedures, yielding results substantially coincident, within the errors due to the discrete numerical approach.

7.1 Energy conservation approach

Due to energy conservation, emissivity is complementary to reflectivity, so that, with reference to q polarization (now $p,q=1,2$ indicate polarization state),

$$
e_q(\theta) = 1-\frac{1}{4\pi}\int_0^{2\pi}\int_0^{\frac{\pi}{2}}\sum_{p=1}^{2}\frac{\sigma^o_{pq}(\theta,\theta_s,\phi_s)}{cos\theta}sin\theta_s d\theta_s d\phi_s \tag{19}
$$

where $\sigma^o_{pq}(\theta,\theta_s,\phi_s)$ is the bistatic scattering coefficient. After discretization, by use of the relation between $\sigma^o_{ij}(\phi_s)$ and $S'_{ij}(\phi_s)$, the properties of the Fourier series yield

$$
e_j = 1-\sum_{i=1}^{2N_\theta}\frac{cos\theta_s sin\theta_s}{cos\theta sin\theta}S_{ij0} \tag{20}
$$

so that only the zero-th order components of functions S_{ij0} are required. This method leads to a procedure which is relatively fast, but does not take temperature inhomogeneities into account.

7.2 Radiative transfer approach

The brightness temperature of the terrain is

$$B_{gj} = e_{gj}\mathcal{T}_g \tag{21}$$

where $\mathcal{T}_g$ is the thermodynamic temperature of the terrain and e_{gj} is its emissivity, which, as shown above, can be given in terms of functions S_{gij0} for the soil. Consider an elementary layer of vegetation at thermodynamic temperature $\mathcal{T}_{v1}$ overlaying the soil. The brightness temperature derives from the superposition of three contributions:

- radiation emitted by the layer towards the upper half-space, B_{11i};
- radiation emitted by the terrain towards the upper half-space and transmitted through the layer, B_{12i};
- radiation emitted by the layer towards the lower half-space, reflected by the terrain, and transmitted into the upper half-space through the layer itself, B_{13i}.

The total brightness temperature is given by

$$\begin{aligned} B_{1i} &= B_{11i} + B_{12i} + B_{13i} \\ &= B_{11i} + \sum_j B_{gj} T^A_{1ij0} + \sum_j B_{11j} S^A_{1ij0} \end{aligned} \tag{22}$$

where

$$B_{11i} = \sigma_{ai} \frac{n\Delta z}{cos\theta} \cdot \mathcal{T}_{v1}, \tag{23}$$

$$\mathbf{S}^A_{10} = \mathbf{T}_0 \mathbf{S}_{g0} (\mathbf{1} - \mathbf{S}_0 \mathbf{S}_{g0})^{-1}, \tag{24}$$

$$\mathbf{T}^A_{10} = \mathbf{T}_0 (\mathbf{1} - \mathbf{S}_0 \mathbf{S}_{g0})^{-1}, \tag{25}$$

and $\mathbf{T}_0, \mathbf{S}_0$, and $\mathbf{S}_{g0}$ are zero-th order Fourier components of the transmission and scattering matrices defined in section 3.1. By combining scattering and transmission matrices, the total scatter matrix of the terrain covered by a single elementary layer of vegetation is obtained. The other N_h elementary layers into which the vegetation canopy is subdivided can now be taken into account by a recursive procedure, provided that $\mathbf{S}_{g0}$ is replaced by $\mathbf{S}_{(k-1)0}$, $\mathbf{B}_{gi}$ by $\mathbf{B}_{(k-1)i}$, and $\mathcal{T}_{v1}$ by the thermodynamic temperature of the succeeding layers $\mathcal{T}_{vk}$, if k denotes the layer which is being added to the previous ones. The $k-th$ iteration gives the brightness temperature of the terrain covered by the first k elementary layers of vegetation and the procedure ends when $k = N_h$. The advantage of this technique consists in its potential in managing non-uniform temperature distributions within the vegetation canopy. Note that in this case the brightness temperature can be computed, whereas the emissivity e is not defined. Only when $\mathcal{T}_g = \mathcal{T}_{v1} = \mathcal{T}_{v2} = ... = \mathcal{T}_{vk} = \mathcal{T}$ the microwave emissivity can be computed from

$$e_i = \frac{B_i}{\mathcal{T}} \tag{26}$$

8 Some numerical results

Selected examples of the results that are obtained by our model are reported in the following, with the main intent of suggesting the kind of analysis allowed by the model and its flexibility.

As is apparent from the preceeding sections, numerous parameters enter the algorithm, and, in particular:

- sensor parameters, i.e., frequency f, off-nadir observation angle θ_0 (azimuthal symmetry of the surface is assumed), polarization p;
- geometric parameters, i.e., soil roughness m, characteristics, dimensions and distribution of orientation of scatterers of various shapes;
- growth parameters, i.e., density ρ_v and height h of vegetation;
- dielectric parameters, essentially dependent on water content, i.e. complex permittivities of ground ϵ_g and of vegetation ϵ_v.

A suitable selection among the various options has been made in order to put into evidence some distinct features of the results. High values of ρ_v and h have been considered so that the contribution from the elements of vegetation is predominant with respect to that from the terrain. The choice of X-band frequency has the same purpose, in addition to the specific relevance of this band for applications (e.g. the SAR-X project [18]). The soil and plants morphological parameters as well as their moisture content correspond to situations typically encountered for agricultural crops in the Mediterranean countries. Random orientation of the scatterers has also been assumed.

Figs. 3 and 5 report the backscattering coefficient σ^o, while Figs. 4 and 6 show the emissivity e of terrain covered with different types of vegetation, modeled as ensembles of 0.2 mm thick dielectric disks (representing plane leaves) and 5 cm long dielectric needles (representing tillers), as functions of the observation angle θ_0 at a frequency of 10 GHz. The canopy is assumed to be 1 m high, the permittivity of the vegetation is $\epsilon_v = 23.3 - j8.7$, and that of the soil $\epsilon_g = 5.5 - j$. The surface of this latter has a mean slope $m = 0.3$. A geometrical optics approximation was adopted.

Discussing in detail the features of the various diagrams is outside the aim of this paper. In summary, we can note the following. When deciduous leaves (modelled as disks) are a major source of scattering, increasing the leaf dimensions makes the dependence of σ^o on θ_0 steeper (Fig.3). This result may be interpreted in terms of more isotropic scattering from small leaves and a more specular one from the large leaves. The effect of the dimensions of the vegetation components can also be appreciated from Fig.4. Indeed, small leaves are associated with a high emissivity and a weak dependence on both θ_0 and polarization. On their side, large leaves are more effective scatterers, so that the emissivity decreases and the difference between polarizations becomes apparent, particularly at higher θ_0. When the vegetation is a mixture of flat leaves (disks) and needles, some distinct differences appear, since the needles decrease the dependence of σ^o on θ_0 and tend to produce more absorption than the disks, thus lowering σ^o (Fig.5). Emission from needles is correspondingly increased (Fig.6) and appears less sensitive to polarization and observation angle. As a general feature, copolar σ^o exhibits opposite trends with respect to e, particularly at low θ_0. This effect,

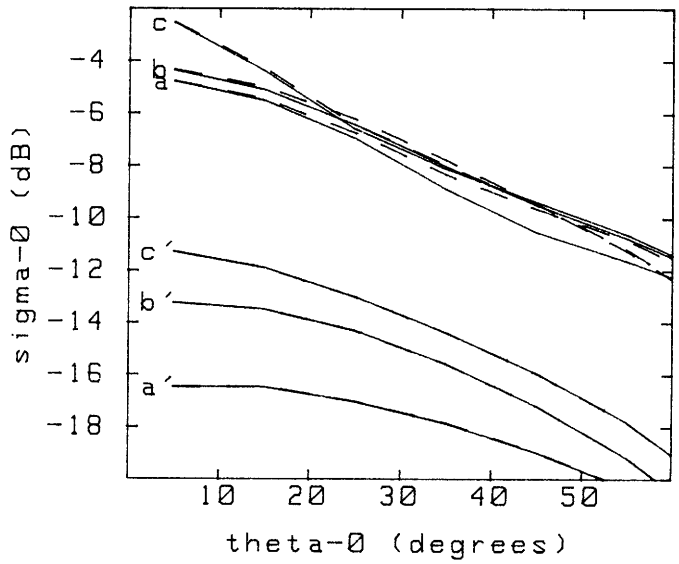

Figure 3: Backscattering coefficient σ^o vs. observation off-nadir angle θ_0 for canopy of circular disks (volume fraction 0.1%) over soil. Curves *a* (radius of disks 0.5 cm), *b* (1 cm), *c* (2 cm): VV polarization (continuous), HH (dashed); *a'* (0.5 cm), *b'* (1 cm), *c'* (2 cm): HV (continuous), VH (dashed). HV and VH curves are superposed.

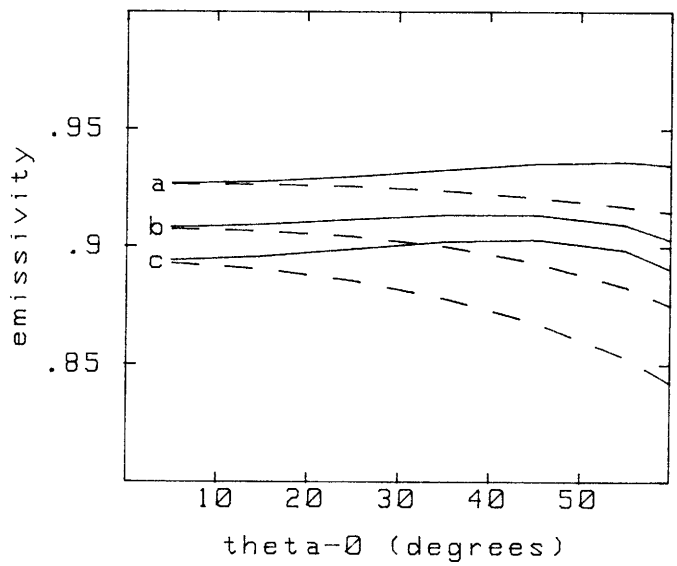

Figure 4: Emissivity *e* vs. observation angle θ_0 for the same disk canopy and parameters as in Fig. 3. Polarizations: V (continuous line); H (dashed line). Disk radius: 0.5 cm (*a*), 1cm (*b*), 2cm (*c*).

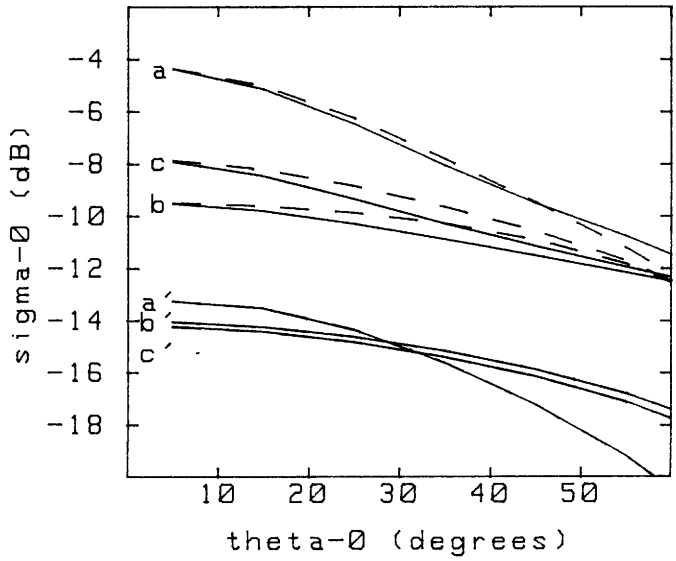

Figure 5: Backscattering coefficient σ^o vs. observation angle θ_0 for three kinds of canopies over soil: disks (curves a,a'), needles (b, b'), mixture of disks and needles (c, c'). Disks: radius 1 cm, volume fraction 0.1 % ; needles: 0.5 mm, 0.4 % , respectively. Polarization state denoted as in Fig. 3.

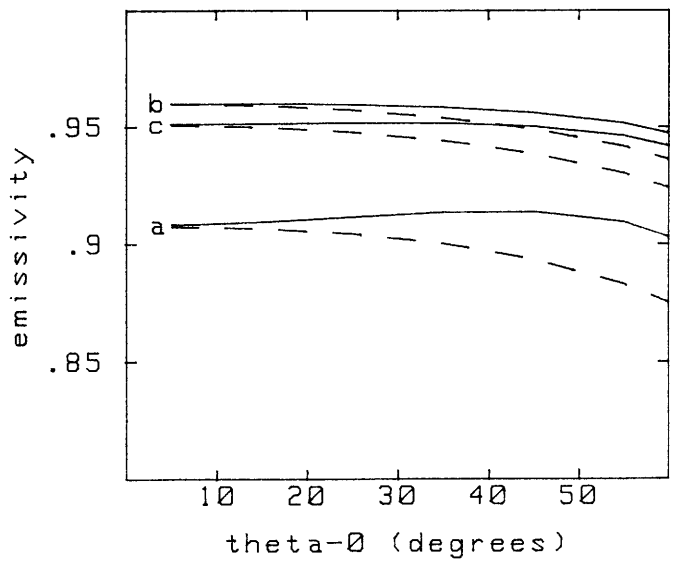

Figure 6: Emissivity e vs. observation angle θ_0 for the same canopies and parameters as in Fig. 5. Polarizations: V (continuous line), H (dashed line). Curve a refers to disks only, b to needles only, c to mixture of disks and needles.

although related to particular configurations of the observed surface, is consistent with the commonly assumed complementarity between radar and radiometric measurements.

The theoretical results produced by the described model can be checked against the experimental data collected in the course of airborne scatterometer and synthetic aperture radar campaigns, such as the ESA/JRC *AGRISCATT* experiment [19]. As an example, Fig. 7 reports σ^o observed at 1.2 GHz together with the values given by the model for different observation angles, averaged over the various fields. The relevant ground data, such as soil moisture content and roughness, plant water content, dimensions and density of leaves, etc., were measured on the various fields and used as input to the model to obtain the theoretical σ^o values for each observation angle. The same quantities, but for the frequency of 13.7 GHz, are reported in Fig. 8. It can be noted that the difference between the average theoretical σ^o values and the ones actually measured on the fields by the airborne scatterometer at both L- and K_u-band is below about 3 dB, while the r.m.s. difference between theoretical and experimental values is found to be 1.8 dB at L-band and 3.1 dB at K_u-band. As a further check, the σ^o yielded by the model lie well within the ranges of experimental values reported in literature [20]. In particular, the theoretical results reported in Fig. 7 are in good accordance with the experimental data shown in the figure of pag. 233 of [20] and those reported in Fig. 8 with the ones in the figure of pag. 253 of [20]. In addition, the numerical model results shown in Fig. 7 of [6] are fairly consistent with the measured data of the figure at pag. 248 of [20].

9 Conclusions

A computational model for microwave scattering and emission from the earth's surface covered with vegetation (*MESCAM*) has been developed and used for estimating the backscattering coefficient and the emissivity. The model is physically based and takes into account multiple scattering both within the vegetation and between vegetation and underlying soil. Because of its characteristics, the model can be used in a wide range of frequencies (typically from L-band to millimeter waves) by a suitable selection of the appropriate scattering functions for the vegetation elements and for the terrain. Sensor parameters and physical quantities directly measurable on the field are needed as inputs, while no additional empirical variable is required. The model has proven to be a rather useful tool for scatterometric, SAR and radiometric data interpretation and validation. In addition, its use allows parametric analyses of emissivity and backscattering both at co- and cross-polarization to study the effects of single soil and vegetation parameters. These effects are difficult to understand by directly interpreting the eventually available experimental data, since, in practice, the measurements are influenced by the contemporary variation of several parameters.

Acknowledgments. Work supported by ASI, Agenzia Spaziale Italiana, and MPI.

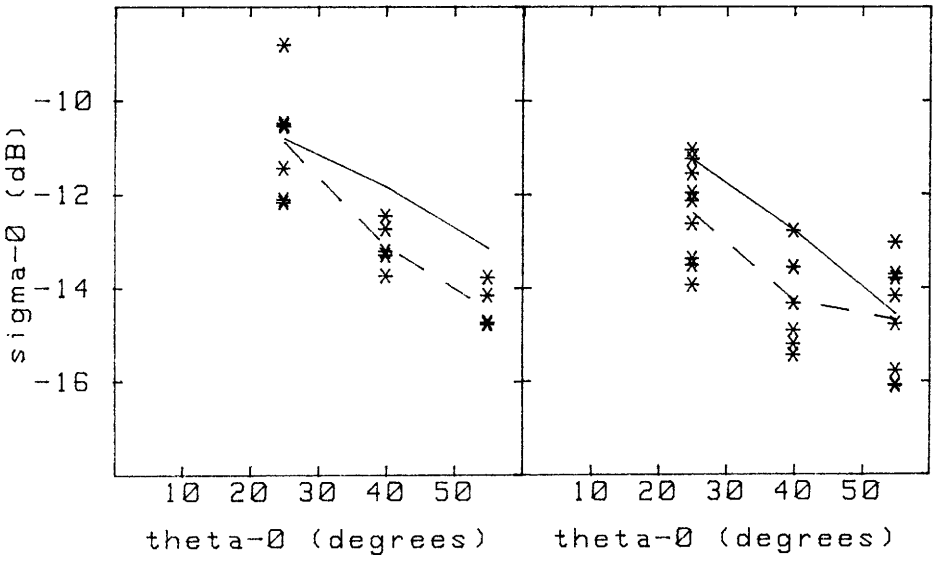

Figure 7: Backscattering coefficient σ^o measured at L-band over sugar-beet fields ($*$: individual samples; broken line: average values) during *AGRISCATT'87* campaign and average theoretical values (continuous line) for three off-nadir angles θ_0 and VV (left) and HH (right) polarizations.

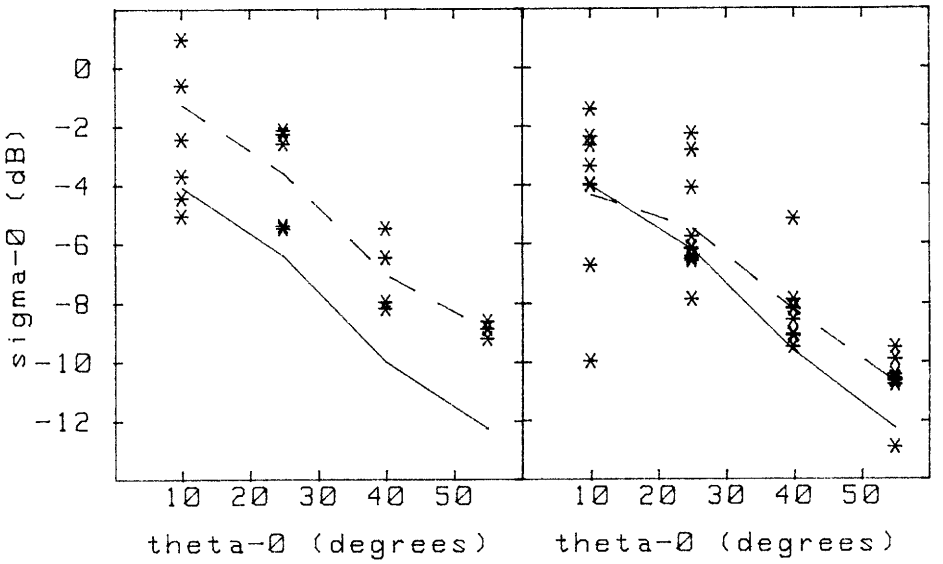

Figure 8: Backscattering coefficient σ^o measured at K_u-band over alfalfa fields ($*$: individual samples; broken line: average values) during *AGRISCATT'87* campaign and average theoretical values (continuous line) for four off-nadir angles θ_0 and VV (left) and HH (right) polarizations.

References

[1] R.H. Lang, and J.S. Sidhu, "Electromagnetic backscattering from a layer of vegetation: a discrete approach", *IEEE Trans. Geosci. Remote Sensing*, Vol. GE-21, pp. 62-71, 1983.

[2] M.A. Karam, and A.K. Fung, "Scattering from randomly oriented circular disks with application to vegetation", *Radio Sci.*, Vol. 18, pp. 557-565, 1983.

[3] H.J. Eom, and A.K. Fung, "A scatter model for vegetation up to Ku-band", *Remote Sensing of Environment*, Vol. 15, pp. 185-200, 1984.

[4] H.J. Eom, and A.K. Fung, "Scattering from a random layer embedded with dielectric needles",*Remote Sensing of Environment*, Vol. 19, pp. 139-149, 1986.

[5] P. Ferrazzoli, G. Luzi, S. Paloscia, P. Pampaloni, G. Schiavon, and D. Solimini, "Comparison between the microwave emissivity and backscatter coefficient of crops" *IEEE Trans. Geosci. Remote Sensing*, vol. 27, pp. 772-778, 1989.

[6] P. Ferrazzoli, G. Luzi, S. Paloscia, and D. Solimini, "Model analysis of backscatter and emission from vegetated terrains", *J. Electromagn. Waves Appl.*, vol. 5, pp. 175-193, 1991.

[7] S. Twomey, H. Jacobowitz, and H.B. Howell, "Matrix method for multiple scattering problems", *J. Atmos. Sci.*, vol. 23, pp. 289-296, 1966.

[8] M.A. El-Rayes, and F.T. Ulaby, "Microwave dielectric spectrum of vegetation - Part I: experimental observations", *IEEE Trans. Geosci. Remote Sensing*, Vol. GE-25, pp. 541-549, 1987.

[9] F.T. Ulaby, R.K. Moore, and A.K. Fung, *Microwave Remote Sensing. Active and Passive, Vol. III, Appendix E*, pp. 2101-2104, Artech House, Dedham, MA, 1986.

[10] L. Tsang, J.A. Kong, and R.T. Shin, *Theory of Microwave Remote Sensing*, pp. 131-135, Wiley, New York, 1985.

[11] J.R. Wait, *Electromagnetic Radiation from Cylindrical Structures*, pp. 142-148, Pergamon Press, New York, 1959.

[12] R. Schiffer, and K.O. Thielheim, "Light scattering by dielectric needles and disks", *J. Appl. Phys*, vol. 50, pp. 2476-2483, 1979.

[13] H.C. Van de Hulst, *Light Scattering by Small Particles*, pp. 69-73, Dover, New York, 1981.

[14] D.R. LeVine, R. Meneghini, R.H. Lang, and S.S. Seker, "Scattering from arbitrarily oriented dielectric disks in the physical optics regime", *J. Opt. Soc. Am.*, vol. 73, pp. 1255-1262, 1983.

[15] F.T. Ulaby, R.K. Moore, and A.K. Fung, *Microwave Remote Sensing. Active and Passive, Vol. II, Chapter 12*, pp. 922-1033, Addison-Wesley, Reading, MA, 1982.

[16] C.E. Nance, A.K. Fung, and J.W. Bredow, "Comparison of integral equation predictions and experimental backscatter measurements from random conducting surfaces", *Proc. IGARSS'90*, pp. 477-480, 1990.

[17] S.L. Broschat, E.I. Thorsos, and A. Ishimaru, "The phase perturbation technique vs. an exact numerical method for random surface scattering", *J. Electromagnetic Waves Appl.*, vol. 3, pp. 237-256, 1989.

[18] H. Öttl *et al.*, *The X-SAR Science Plan*, DFVLR Mitteilung 85-17, 1985.

[19] E. Attema, "Radar signature measurements during the *AGRISCATT* campaigns", *Proc. IGARSS'88*, (Edinburgh, U.K.), ESA SP-284, pp. 1141-1144, 1988.

[20] F.T. Ulaby, and M.C. Dobson, *Handbook of Radar Scattering Statistics for Terrain*, Artech House, Norwood, MA, 1989.